

# Regenerative and non-regenerative transcriptional states of the human epicardium: from foetus to adult and back again: Supplementary Figures

Vincent R. Knight-Schrijver<sup>1</sup>, Hongorzul Davaapil<sup>1</sup>, Alexander Ross<sup>1,2</sup>, Xiaoling He<sup>1,3</sup>, Ludovic Vallier<sup>1</sup>, Laure Gambardella<sup>1\*+</sup>, and Sanjay Sinha<sup>1\*+</sup>

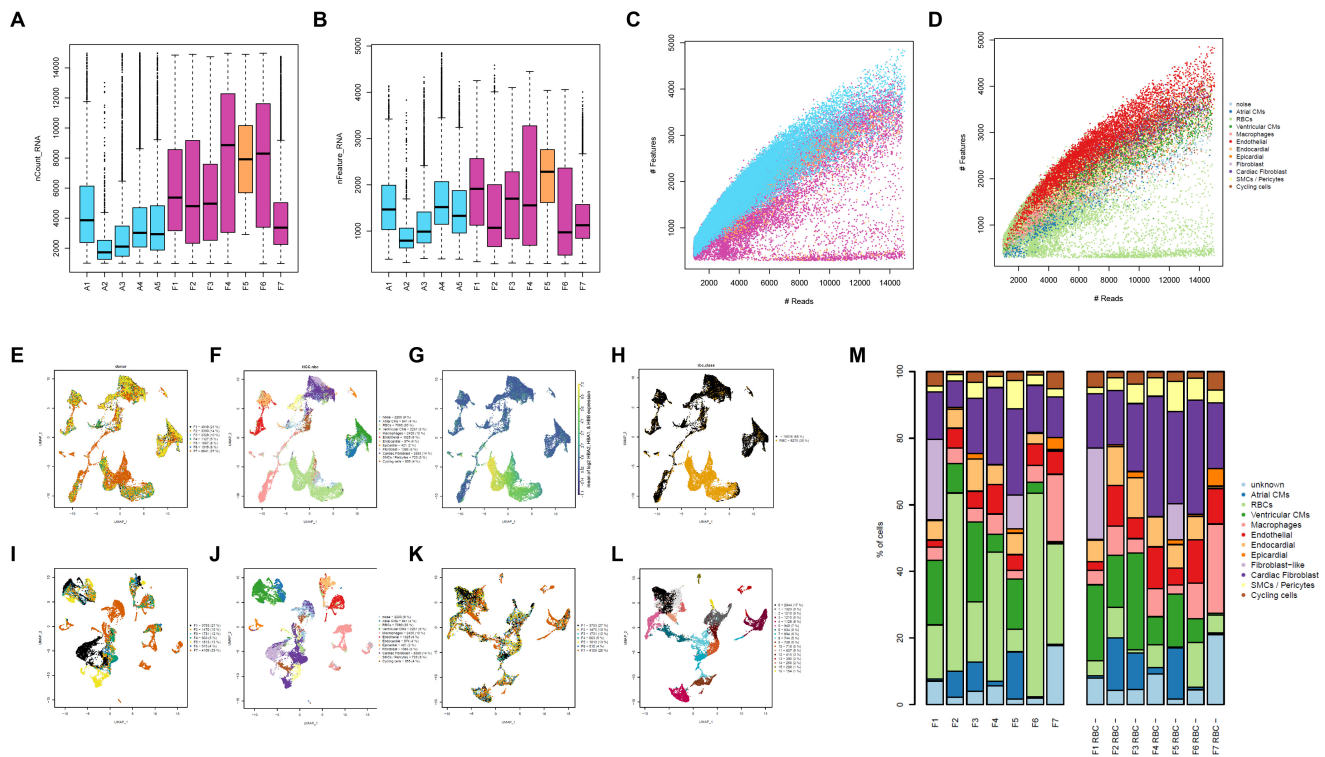
<sup>1</sup>Wellcome-MRC Cambridge Stem Cell Institute, Jeffrey Cheah Biomedical Centre, Cambridge Biomedical Campus, University of Cambridge, Puddicombe way, Cambridge CB2 0AZ, UK

<sup>2</sup>Department of Surgery, University of Cambridge, Cambridge CB2 0QQ, UK

<sup>3</sup>John van Geest Centre for Brain Repair, Cambridge University, Cambridge, UK

\*Corresponding author addresses: LG lg231@cam.ac.uk, SS ss661@cam.ac.uk

+Co-senior authors



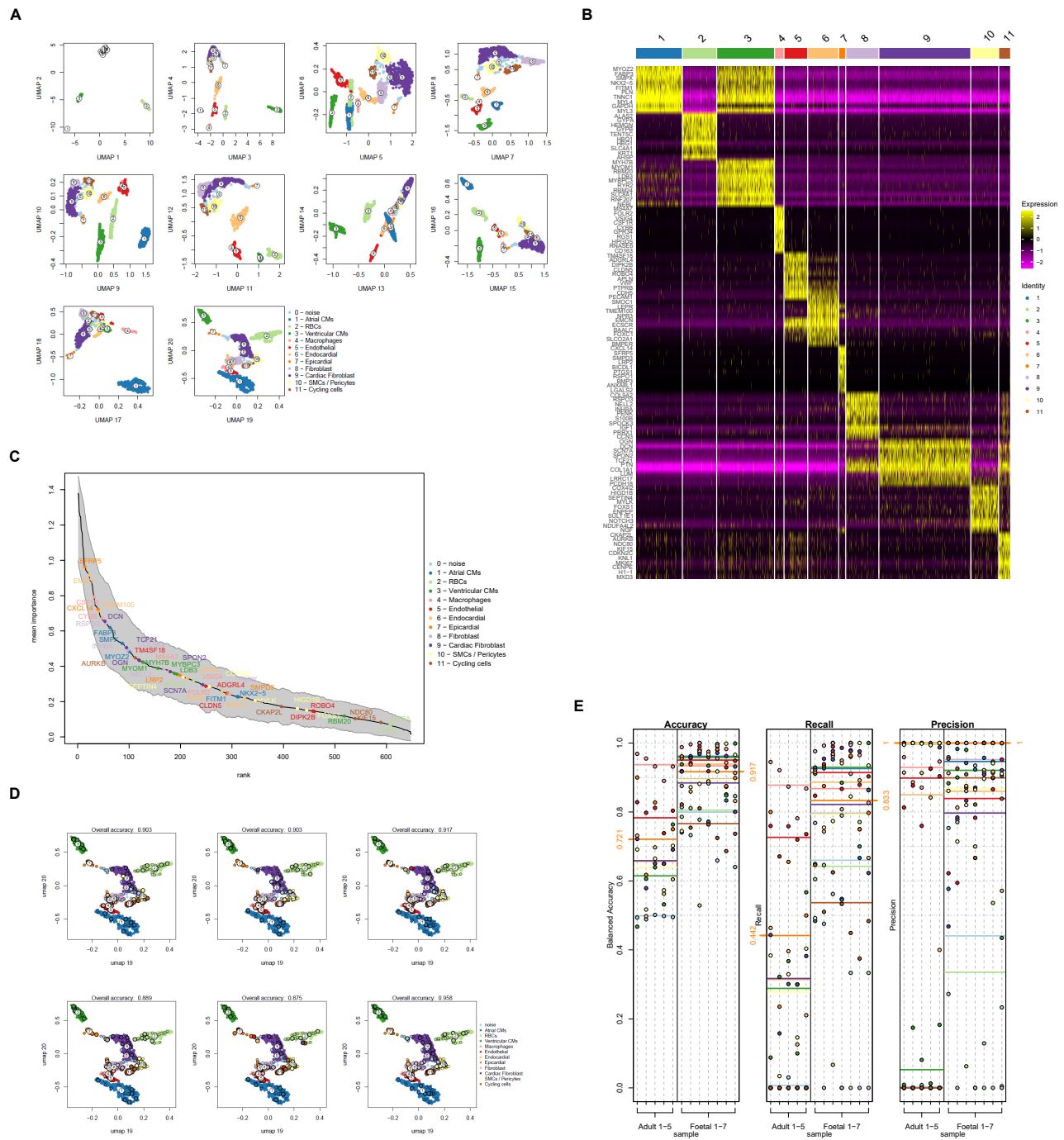


**Figure 2.** **A**, The first 20-components of a 50-dimensional uniform manifold approximation and projection (UMAP) of the gene-frequency matrix from sample F5 labelled by the 12 HDBSCAN clusters; **B**, top 10 gene markers for each HDBSCAN cluster identified using Wilcoxon ranked sum tests, of which the top 5 are located in; **C**, the ranking of gene features by the importance parameter from a random-forest feature optimization approach; **D**, UMAP components 19 and 20 with showing sampled cells belonging to each fold of cross-validation (small circle) as well as predictions (larger circle); and **E**, the accuracy, recall and precision of the classifier in all datasets determined independently by assessing the classifier’s ability to capture cells belonging to putative clusters after within-stage integration of samples.

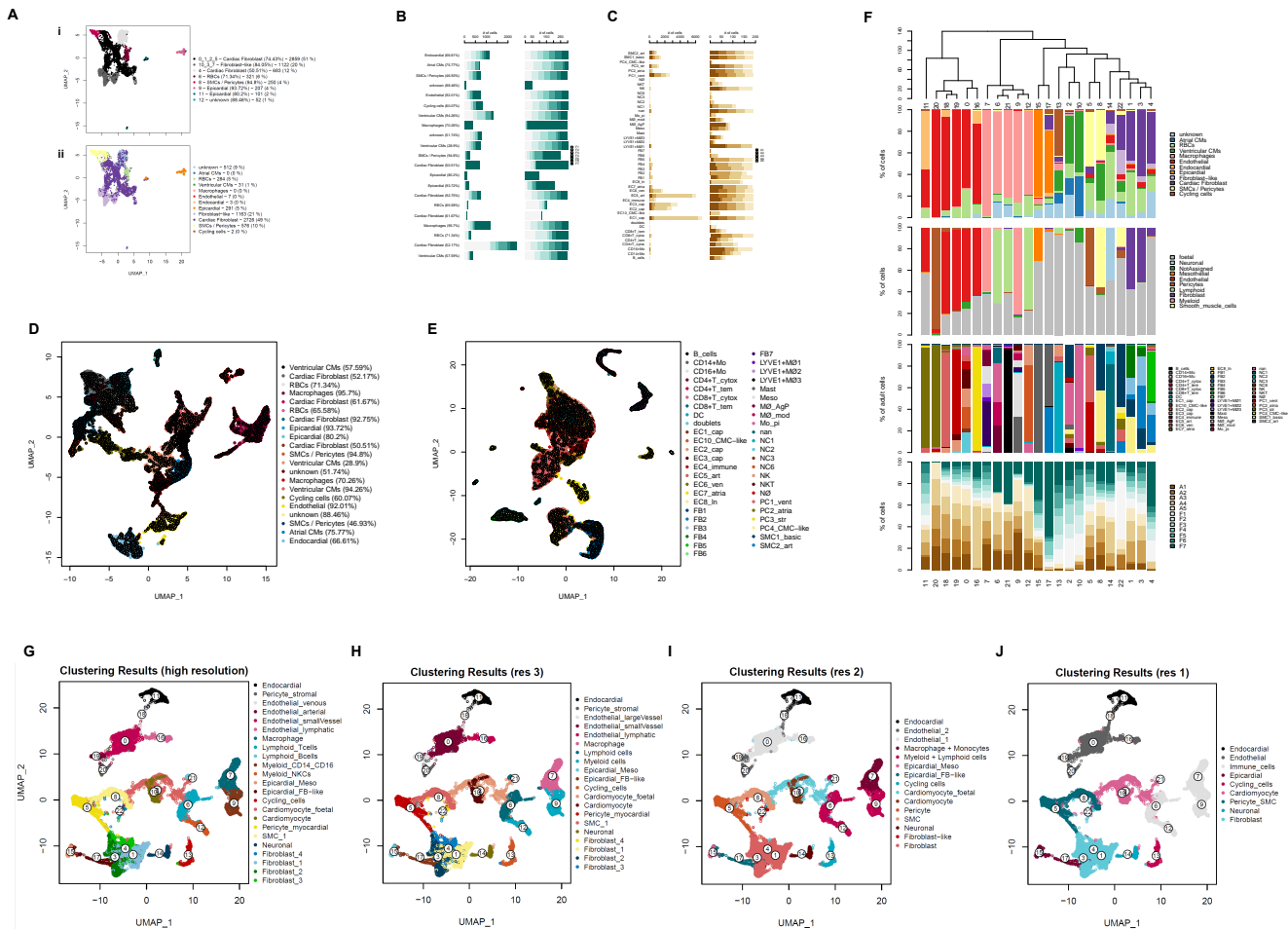


**Figure 3.** Stratified subsampling of datasets carried out by **A**, sub-clustering of epicardial, fibroblast and smooth muscle cell clusters identified in the foetal-integrated dataset; **B**, equally sampling of foetal clusters across donors and clusters to generate new equally-distributed foetal samples; **C**, equally sampling of adult “cell.states” across donors to generate new equally-distributed adult samples; **D**, umap of integrated foetal samples showing the locations of sub-sampled cells; **E**, umap of integrated adult samples showing locations of sub-sampled cells, **F**, highest resolution clusters for the integrated dataset after stratified sub-sampling ordered by hierarchical clustering of HCC-class compositions. Bar charts show a number of annotations types including HCC-class distribution, HCA-derived labels for adult cells (*cell.types* and *cell.states*) as a fraction of adult cells, and the distribution of the different samples among the clusters; **G-J**, decreasing resolutions of clustering in the integrated dataset after stratified sub-sampling.



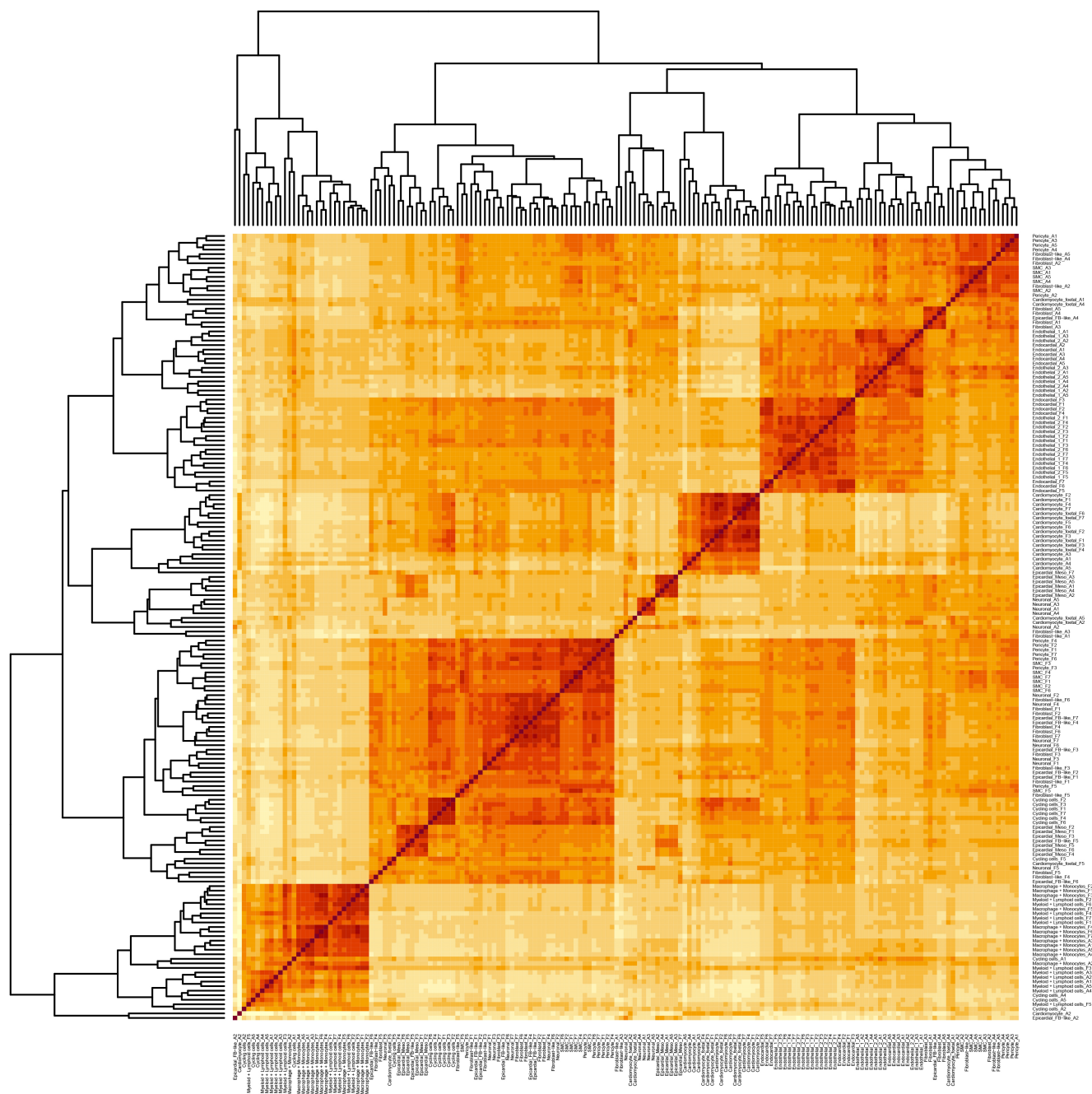


**Figure 5.** Pseudobulk downsampling of all cell types across adult and foetal donors and the results of hierarchical clustering.

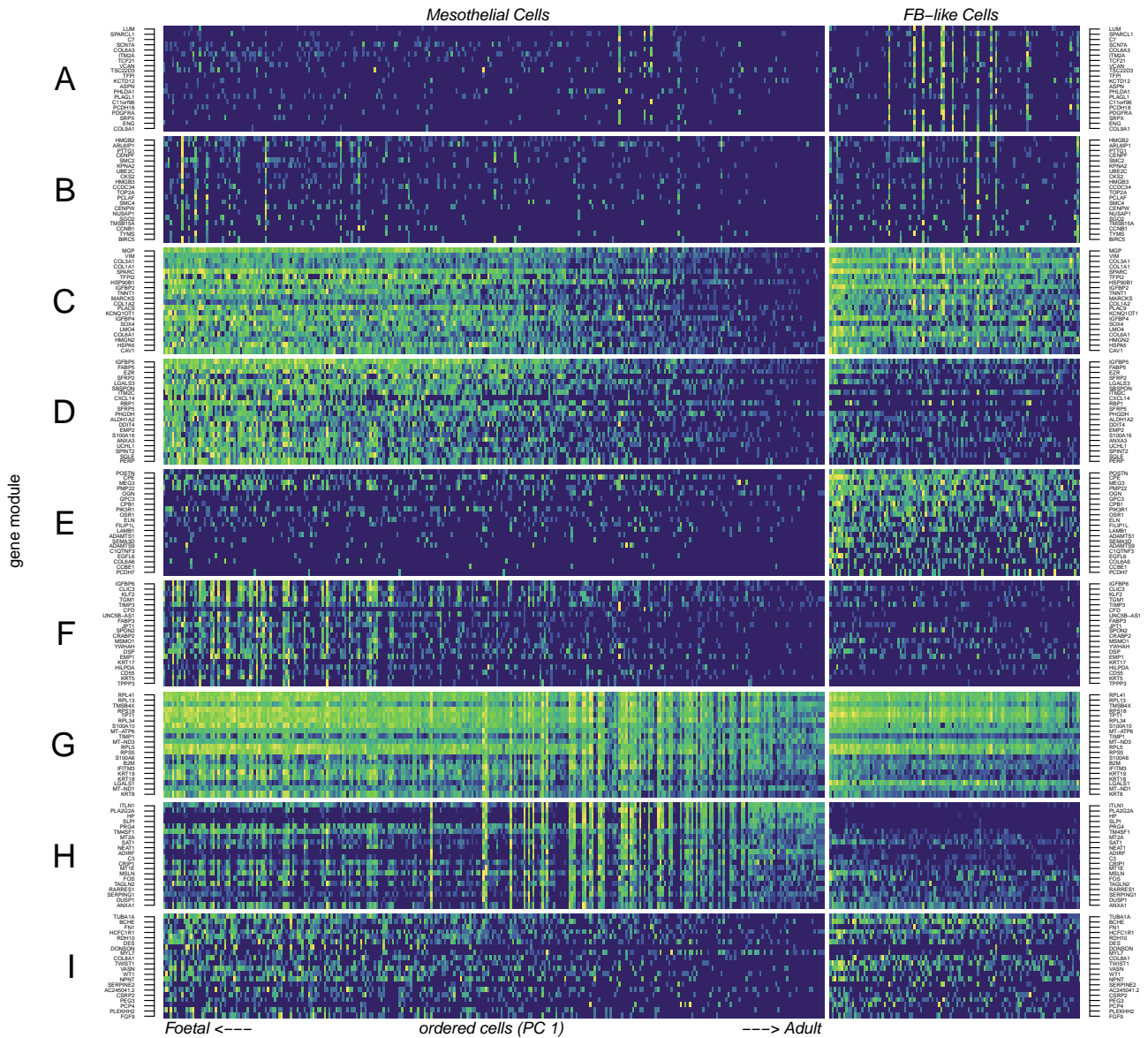


**Figure 6.** Gene module principal component analysis shows an age-associated switch in gene module commitment seen with ordering all epicardial cells by principal component 1 coordinates. The top 20 genes by expression were sampled from each module and shown here.